Marine Structures 24 (2011) 275–291

Contents lists available at ScienceDirect

Marine Structures

journal homepage: www.elsevier.com/locate/marstruc

A finite element model for flexible pipe armor wire instability

M.A. Vaz*, N.A.S. Rizzo

Ocean Engineering Program, Federal University of Rio de Janeiro, P.O. Box 68508, 21945-970 Rio de Janeiro, RJ, Brazil

ARTICLE INFO

Article history:
Received 1 October 2010
Received in revised form 21 February 2011
Accepted 4 March 2011

Keywords:
Flexible pipe
Armor wire instability
Birdcaging

ABSTRACT

The constructive disposition of metallic and plastic layers confers flexible pipes with high and low axial stiffness respectively when tensile and compressive loads are applied. Under certain conditions typically found during deepwater installation or operation, flexible pipes may be subjected to high axial compression, sometimes accompanied by bending. If not properly designed, the structure may not be able to withstand this loading and fails. From practical experience observed offshore and in laboratory tests two principal mechanisms, which will be discussed in this paper, have been identified regarding the configuration of the armor wires. When the pipe fails by compression the armor wires may exhibit localized lateral or radial deflections, consequently permanent damage is observed in the armor wires with a sudden reduction of the structure's axial stiffness. The pressure armor may also unlock, thus causing potential fluid leakage.

In this work a finite element model is developed to estimate the critical instability load and failure modes. An axi-symmetric model is constructed employing a complex combination of beam and spring elements. For each armor layer only one wire needs to be modeled, hence the computational cost is minimized without compromising the phenomenon characterization. A parametric case study is performed for a typical flexible pipe structure, where the friction coefficient between the wire armors and the external pressure are varied, and the critical instability loads and failure modes are obtained and results are discussed.

* Corresponding author. Tel.: +55 21 25627062; fax: +55 21 25628803.
E-mail address: murilo@peno.coppe.ufrj.br (M.A. Vaz).

0951-8339/$ – see front matter © 2011 Elsevier Ltd. All rights reserved.
doi:10.1016/j.marstruc.2011.03.001

1. Introduction

Flexible pipes are tubular composite structures, consolidated by the juxtaposition of concentric cylindrical polymeric layers and metallic wound wires. They work together but independently thus offering strength and leak-proof structure without compromising the required flexibility. They have been widely employed by the oil & gas industry in offshore applications in the last decades. The flexible pipe structure is basically composed by an interlocked stainless steel carcass that resists the external pressure, polymeric layers that offer fluid leak-proof capacity and reduce the wear between the metallic layers, a steel pressure armor that resists the internal pressure, usually two tensile armors helically wound in opposite directions to provide strength and an anti-birdcaging tape that reduces the radial expansion from the tensile armors, see Fig. 1a.

Flexible pipes are designed to withstand high tensile loads, nonetheless significant compressive loads may be also experienced during deepwater installation (end-cap effect due to high hydrostatic pressure) or in extreme situations such as when the floating unit operates in near conditions (top low angle) and is subject to severe motions. In such conditions an instability phenomenon may take place and the armor wires may experience large lateral or radial displacements, this latter being usually referred as birdcaging because of the assumed topology of the wires. Unfortunately, only a few papers have been published on this subject, given the complexity to develop analytical or numerical models and cost involved in performing experiments. It is known that manufacturers and some operators have carried out a few tests, but results have not been made public nor have been reliably compared with predictive formulations.

Birdcaging is a phenomenon also reported in steel cables. Costello [4] advocated that a compressive load or a combination of axial load and moment may cause the formation of wire birdcaging and suggested as a criterion that loss of contact between the strands should be avoided. Stump & Heijen [10] propounded a procedure where the helix curvature may be considered as an initial imperfection.

Braga [3] carried out mechanical tests in short samples of flexible pipes applying monotonic and cyclic compressive and bending-compressive loads. The results of the tests indicated that there was a substantial loss in strength when cyclic loads were applied. The author credited this reduction to the deterioration of the anti-birdcage bandage due to wear, however this possibility was not systematically investigated. Unfortunately, the physical and geometrical properties of the samples of flexible pipes tested were not informed. Zhang et al. [14] developed a finite element model for the design of flexible pipes against radial expansion. Experimental validation was said to have been performed, however very little information was actually available regarding either the numerical model or the experimental tests. Bectarte & Coutarel [2] discussed a methodology to predict the lateral instability based on extensive testing in laboratory and during expensive offshore campaigns (Deepwater Immersion Performance Test – DIP). Again there was no information of the characteristics of the structures tested, failure modes or loads. Sousa [9] presented a simplified finite element model where the armor wires were represented by a single wire resting on a non-linear foundation. Custódio [5] proposed a complex analytical model for estimation of the instability of armor wires by applying a perturbation method on the governing equations of a slender spatial wire thus yielding an eigen-value problem. Tan et al. [11] developed a model based on the total strain energy to describe the buckling and post-buckling behavior of the tensile wire armors and calibrated results against experimental data obtained from DIP tests. Again both model and results were not clearly presented. The American Petroleum Institute recently reviewed the standard [1], but this failure mechanism was basically just defined, methodology and criteria were not presented.

Birdcaging, schematically shown in Fig. 1a, is an instability mechanism that takes place when the armor wires predominantly displace in the radial direction. This failure mode usually occurs when the

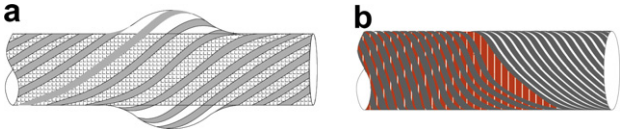

Fig. 1. Schematic representation of the radial and lateral instabilities, respectively.

external sheath is damaged and the annulus is wetted because in this condition the external pressure does not support the expansion of the armor wires, even though the axial compressive load diminishes. To avoid this failure mode the flexible pipe may be manufactured with high stiffness and high strength tape (e.g., E, S-2, Kevlar®, AS4, P100S and IM8) to support the armor layers.

The anti-birdcage tape may avoid the radial instability, however a lateral type instability may be triggered, see Fig. 1b. Novitsky & Sertã [7] suggested two possible failure modes associated to lateral instability:

- *Dry annular* – when the external plastic layer is intact and the lateral displacement of the armor wires is impeded by high friction, high compressive stresses are built and failure may be elasto-plastic.
- *Wet annular* – when the external plastic layer is damaged the friction forces substantially reduce hence failure is more likely to be elastic.

This paper presents, in detail, the development of a complex finite element model that predicts the critical load and the morphology of the wires after instability. It also demonstrates how radial and lateral tensile armor wire instability may occur. A case study is presented for a 9.5″ flexible riser and the influence of the external pressure and the friction coefficient between the armor wires on the instability load and mode for flooded and non-flooded annulus is investigated. The results from the parametric analysis are consistent with experimental data reported in literature.

2. The finite element model

A non-linear static finite element model is developed to simulate the flexible pipe armor structural instability. The software Abaqus [6] is employed. The model aims to represent the flexible pipe cross-section structural behavior as accurately as possible without penalizing the computational time.

The model is basically composed by two wires representing the internal and external tensile armors resting on non-linear elastic foundations, thus depicting the complex interaction between the wires and all other layers. The geometric properties of the equivalent wires are proportional to the number of wires in each layer and the elastic foundation of each equivalent wire is represented by non-linear springs. The internal wire foundation only resists inward radial displacement provided by the internal layers (e.g., interlocked carcass, internal plastic sealing layer, pressure armor and anti-wear plastic layer). The external armor wire is connected to a non-linear spring that solely provides strength against radial expansion (the wire is free to contract), representing the stiffness of the most external layers (e.g., the anti-birdcage tape and external plastic layer).

As the wires are contra-helicoidally wound, it is possible to represent their contact by modeling a cylindrical surface without stiffness coupled to one of the equivalent wires, hence ensuring that they move together. In the model developed in this paper the cylindrical surface was coupled to the external wire.

The axial and torsional stiffness of the polymeric layers are low, but they can be easily modeled at practically no computational cost as a beam localized in the pipe axis with equivalent properties. The axial and torsional stiffness from the carcass and pressure armor were not considered because they are negligible in fact. A schematic drawing of the proposed model is presented in Fig. 2.

A general view of the model is presented in Fig. 3, illustrating the finite element mesh employed with three helical pitches of the external armor wire. The mesh is composed by beam (B31), spring (SPRINGA), surface (SFM3D4) and connection (CONN3D2) elements respectively employed to model the equivalent armor wires, the radial elastic support from remaining layers, the contact between the equivalent wires and the connection between the pipe ends and the equivalent armor wires.

The contact between the two wires is modeled with a cylindrical surface without stiffness and with the same radius as the internal wire. This artifice was crucial for the success of the model with only two wires, and enabled an inexpensive simulation. The cylindrical surface plays the role of the full external armor wire layer that may contact the equivalent internal wire. Hence, even though the internal and external armor wires are respectively represented by only one equivalent wire, adequate contact can be captured by this model.

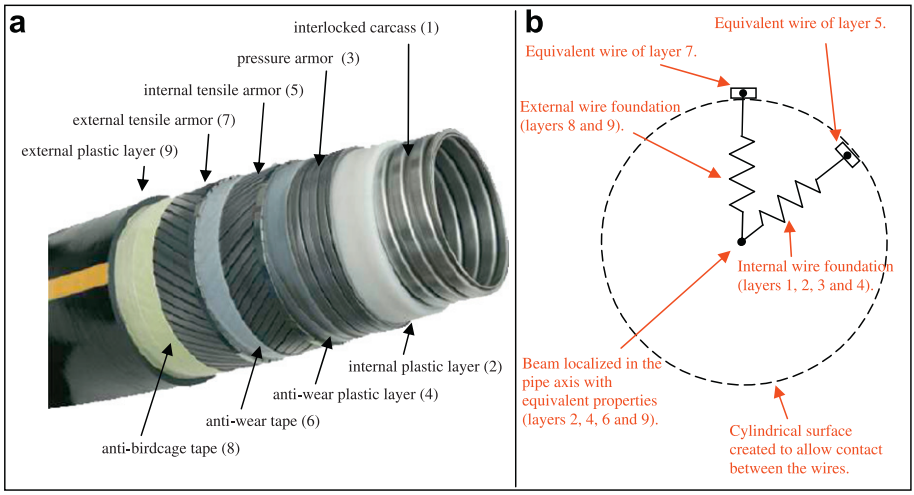

Fig. 2. (a) Typical Flexible Pipe; (b) Schematic representation of the proposed model.

Fig. 4a illustrates the behavior of the wires under an axi-symmetric load and it can be seen that only one wire needs to be represented to obtain the layer configuration, because the wires respond axi-symmetrically. The node of a certain wire cross-section is the master and the other ones are slaves, that is, the slave nodes cyclically follow the master node. The cylindrical surface of the model is formed by n_{dv} cross-sections which are "slaves" of the respective external wire node with n_{dv}/n_p (Fig. 4b) nodes in each cross-section (where n_p is the number of pitches in the model). It is important to note that the nodes of the cylindrical surface do not have any degree of freedom due to their cyclic symmetry hence the computational cost does not depend on the surface refinement.

The equivalent wires have different radii, hence the cylindrical surface is modeled with the same radius as the contacting surface (i.e., the radius of the equivalent wire for the internal armor) to correctly account for the contact, as can be seen in Fig. 5.

The anti-wear tape is modeled by reducing the friction coefficient between the armor wires. In summary, the contact is characterized by:

- Interaction between the cylindrical surface and the equivalent internal armor;
- Small or finite sliding;
- Surface to surface contact;

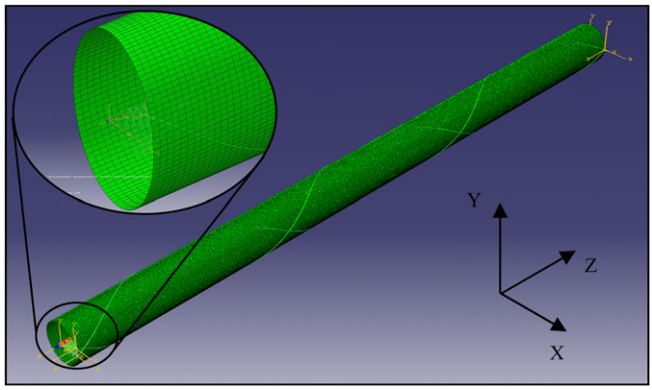

Fig. 3. General view of the finite element model.

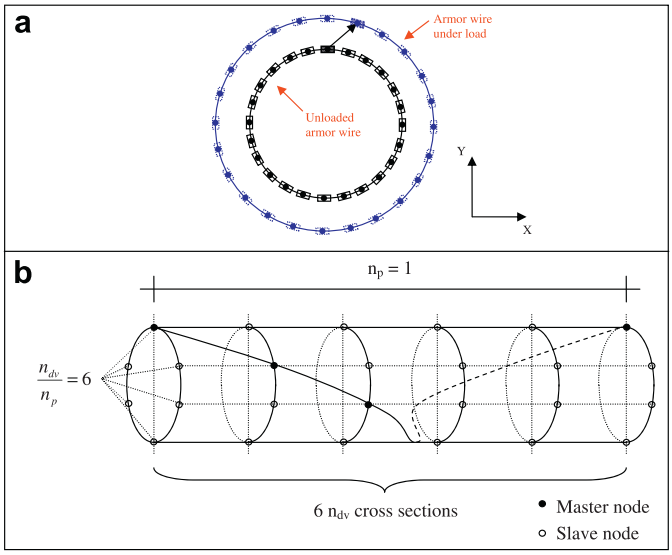

Fig. 4. Schematic representation of (a) behavior of armor wires under axi-symmetric loading; (b) n_{dv}/n_p parameter.

- Mohr–Coulomb Friction coefficient;
- Gap simulation between the armors.

As the internal and external wires are laid on a cylindrical surface and are not allowed to freely rotate (see Fig. 6), a constraint was created in the model that radially fixes the direction of the principal coordinates.

The loading is carried out in two steps: firstly the external pressure is applied on the cylindrical surface and secondly compression is imparted to the wires' ends. Direct application of a compressive axial load yielded localized bending near the wire ends hence displacement increments were imposed in the helix direction. The axial compressive force F_Z is related to the reaction forces that arise from the controlled displacements, respectively $f_{Z,i}$ and $f_{Z,e}$ for the internal and external armors:

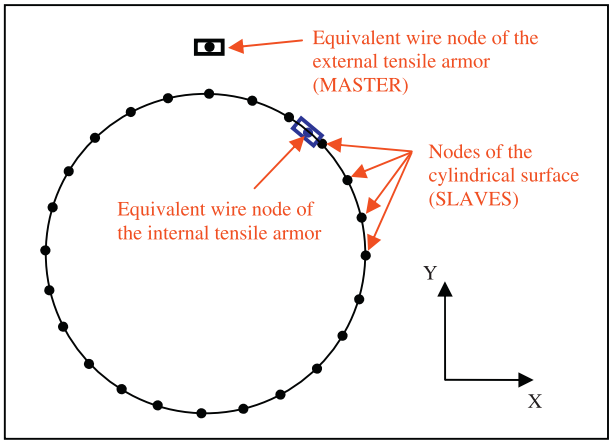

Fig. 5. Master and slave nodes for cyclic symmetric cross-section.

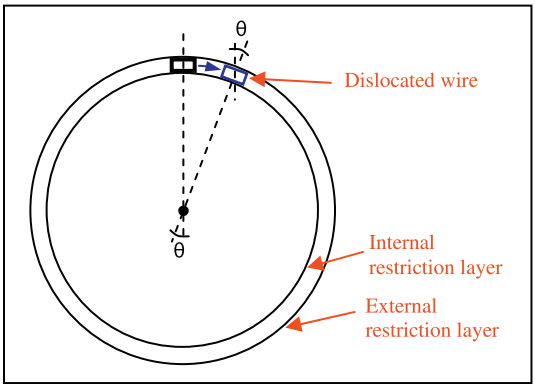

Fig. 6. Motion constraint for the equivalent wires.

$$F_z = \frac{f_{Z,i}}{\cos^2(\alpha_i)} + \frac{f_{Z,e}}{\cos^2(\alpha_e)} \tag{1}$$

where α_i and α_e are respectively the laying angles for the internal and external wires. It should be mentioned that the displacement controlled loading in the helix direction does not totally avoid local bending but their influence on the global response is minimum.

The problem addressed in this research involves a highly unstable phenomenon, where the structure would "dynamically" assume a new equilibrium configuration far from the initial condition. For the solution of this class of problem ABAQUS offers an automatic mechanism that is triggered by the inclusion of the STABILIZE parameter. This procedure introduces "spurious" viscous damping forces into the global equilibrium equations therefore it must be used with caution. The forces artificially introduced in the system should be small enough to avoid significant change of the response while the structure is stable and should be large enough to dissipate the strain energy when the structure instabilize.

The nodes from the elastic foundations that belong to the axis of revolution are not allowed to move in the *X* and *Y* directions (Fig. 3). In addition, both nodes from each spring are coupled in the *Z*-direction to ensure that only radial forces are built.

To facilitate the finite element meshing a FORTRAN® pre-processor code was developed. In summary the model encompasses the following features:

- Basically beam and non-linear spring elements are employed, which makes the analysis computationally light.
- The formulation considers geometrical nonlinearities.
- Material nonlinearities may be also included.
- Monotonic loading (displacement) is employed.
- Loss of contact, gaps and friction between the armors may be simulated.
- Finite sliding of the armors is allowed.

The effect of initial imperfections and residual stresses are mostly often detrimental to the instability load capacity of structures but they were not considered in this paper.

3. Case study

Initially the model was employed to an axi-symmetric structural analysis of a 2.5″ flexible pipe submitted to tensile and torsion loadings as presented by Witz [13], where experimental data and analytical results from several organizations were compared. The results presented by Rizzo [8] show that the FEM developed here is also able to satisfactorily capture the axi-symmetric response.

A 9.5″ flexible pipe structure [9] was chosen for the instability analysis. There are 74 armor wires in the internal and external layers, laid at 30° with respect to the pipe generatrix. The helix radii are 299.3 and 305.3 mm, respectively. The rectangular cross-section for both wires is 3 × 10 mm and is built with high strength carbon steel with yield and rupture stresses respectively equal to 1100 MPa and 1500 MPa.

The anti-birdcaging tape thickness, modulus of elasticity and rupture stress are respectively equal to 2.4 mm, 35000 MPa and 261 MPa. The contribution from the external plastic sheath on the radial elastic foundation was not considered. A non-linear spring was adopted to represent the behavior of the anti-birdcaging tape with yield stress σ_{kev}^{esc} adopted equal to the rupture stress. If the tape is assumed a thin cylinder submitted to uniform internal pressure resulting from the expansion of the external wires, the yield spring force N_{mol}^{esc} is given by (Young, 1990):

$$N_{mol}^{esc} = \frac{\sigma_{kev}^{esc} \cdot A_{cont} \cdot h_{kev}}{R_{kev}} \tag{2}$$

$$A_{cont} = \frac{2 \cdot \pi \cdot R_7 \cdot L_{mod}}{n_{dv}} \tag{3}$$

where R_{kev} and h_{kev} are respectively the tape radius and thickness, R_7 is the radius of the external wire, L_{mod} is the length and n_{dv} is the number of divisions of the model.

To avoid the influence of the ends in the results it was considered that only the central springs located up to 1/30 of the total model length could yield. Given the lack of information, the radial stiffness of the layers 1–4 (interlocked carcass, pressure armor and plastic layers) was assumed proportional to the 2.5″ pipe described by Witz [13], hence the stiffness is equal to 5×10^6 N/mm. That stiffness value is only important for intact structures where the external pressure acts directly on the wires. The properties of the anti-birdcaging tape are found to be of paramount importance for the instability analysis. The properties of the polymeric layers were not considered as they play an insignificant role in the phenomenon.

Parametric analyses were performed varying the friction coefficient between 0 and 0.4 and the external pressure between 0 and 15 MPa, which is approximately the hydrostatic pressure at the operating water depth of 1500 m.

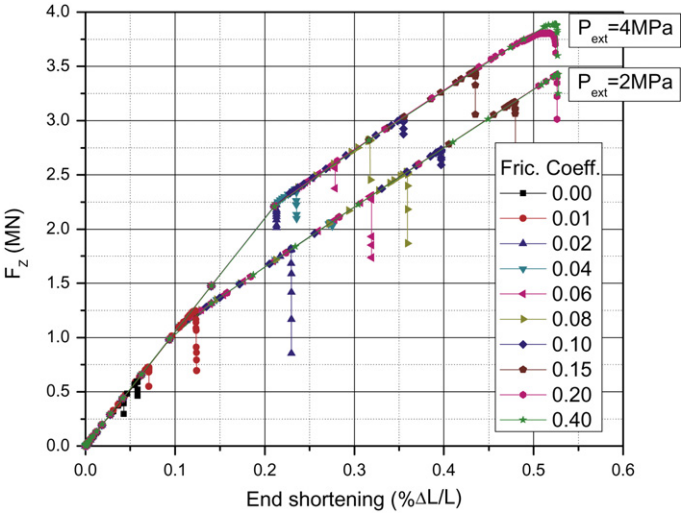

Fig. 7. Compressive load versus end shortening (Pext = 2 and 4 MPa).

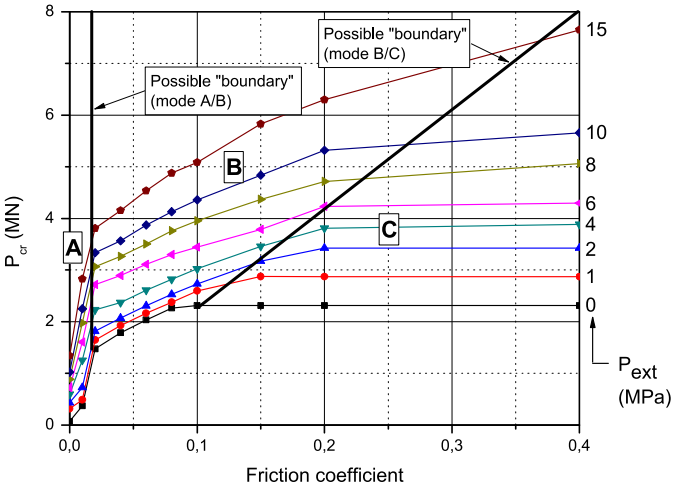

Fig. 8. Instability load versus friction coefficient for several external pressures.

The instability load P_{cr} is obtained as the maximum load supported by the structure when displacements are imposed. When the armor wires instabilize the load suddenly drops. Fig. 7 shows the relationship between the compressive load F_Z and the end shortening $\Delta L/L$ for several friction coefficients and external pressures equal to 2 and 4 MPa. It is observed that the curves' inclination reduce when the end shortenings are near 0.1 and 0.2% respectively for external pressures equal to 2 and 4 MPa. The change in stiffness arises because, for higher compressive loads, the wires overcome the external pressure P_{ext} and then are able to lay on the anti-birdcaging tape elastic foundation.

Fig. 8 shows the instability load as a function of the external pressure and friction coefficient. It is seen that initially the inclinations of the curves are sensitive to the friction coefficient but from a certain value (approximately 0.02) the inclination drops for all external pressures. When the friction coefficient is further increased the critical load tends to stabilize, especially faster when the external pressure is reduced. This behavior is intimately related to the instability mode. It was observed that the initial high gradient is related to a lateral instability mode where each equivalent wire instabilizes independently. This mode is denominated MODE A. When the inclination reduces the equivalent wires behave as a unique layer but instability is also lateral. This mode is called MODE B. When the curves reach a plateau a new instability mode takes place, predominantly radial, or birdcaging, denominated MODE C. The horizontal behavior is justified by the fact that the anti-birdcaging tape has failed so the load is independent of the friction coefficient. A fourth radial instability mode, called MODE D, has been identified, but is not clearly seen in the case study presented here. This mode is apparently initiated with the spatial buckling of the armor wires in the elastic foundations. As more load is applied, the "wrinkling" and the average radial displacement of the equivalent wires simultaneously progress and failure criteria may be associated with the strain condition within the wire or with the rupture of the anti-birdcaging tape. The instability MODE D has been observed for high friction forces between the equivalent armors, i.e. for high friction coefficients and high external pressures.

Next, the instability modes are addressed in details.

3.1. Lateral instability, MODE A

To discuss this case two examples were chosen with friction coefficient equal to 0.01 and external pressures equal to 6 and 15 MPa (cases 1 and 2) since they are quite far away from MODE B that should occur for a friction coefficient near 0.02. Fig. 9 shows the model configuration (radial scale factor equal

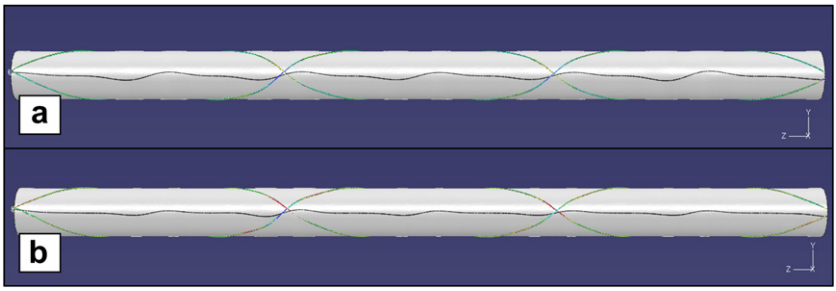

Fig. 9. Riser configuration with friction coefficient equal to 0.01 and external pressures equal to (a) 6 MPa and (b) 15 MPa.

to 5) when the structure instabilizes. The model was built with a "line" in the cylindrical contact surface so a circumferential (lateral) structure displacement could be detected.

Fig. 10 shows the wire rotation in the pipe axial direction as a function of the pipe length when the structure instabilizes. It is shown that each armor wire is free to rotate independently and the average rotation is zero and a peak occurs at the left/right sides due to the end conditions. In addition the wires seem to instabilize at a wavelength equal to $L_p/2$ independently of the external pressure. In summary it can be said that the contact pressure between the armor wires is insufficient to ensure that both layers will instabilize together. The friction force is not high enough hence each wire can instabilize in any direction.

3.2. Lateral instability, MODE B

To illustrate this instability mechanism cases 3 and 4 are chosen with friction coefficient equal to 0.04 and external pressures respectively equal to 6 and 15 MPa. Fig. 11 presents the flexible pipe configuration (radial scale factor equal to 10) just after the structure instabilizes. The instability is not obviously lateral, even though it is evident that it is not radial. However, it is easy to perceive (by observing the line in the cylindrical surface) that the displacements caused by the boundary conditions are much larger than the circumferential displacements of the wires, characterizing this mode of instability.

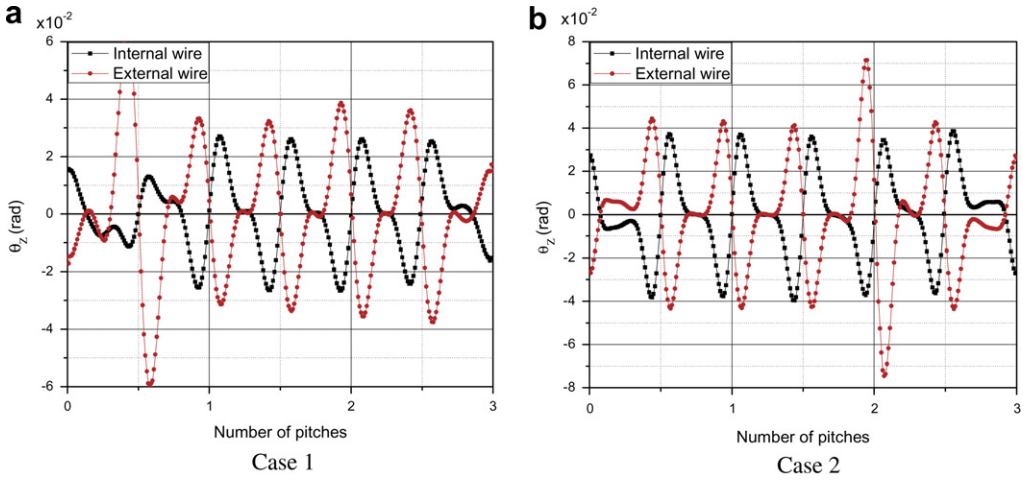

Fig. 10. Rotation around the axis Z as a function of the model length.

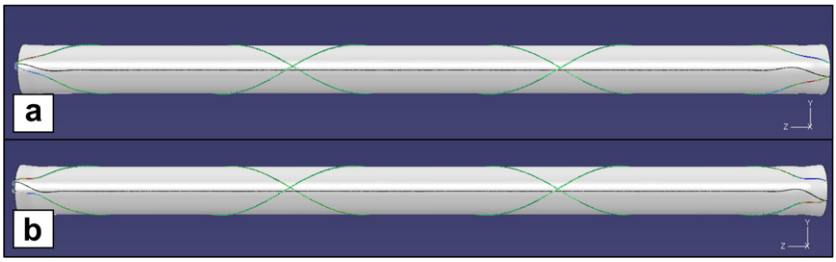

Fig. 11. Riser configuration with friction coefficient equal to 0.04 and external pressures equal to (a) 6 MPa and (b) 15 MPa.

The instability mode is seen in Fig. 12, which shows the wire rotation in the pipe axial direction as a function of the pipe length when the structure instabilizes. It is noted that the rotation distribution along the wire resembles the one from MODE A. However, in MODE B both wires rotate much less (around 100 times less) and exhibit a non-zero average rotation, which grows with the external pressure, indicating that the armor wires instabilize together.

3.3. Radial instability, MODE C

The radial instability (MODE C) is experienced in this case study for a friction coefficient 0.40 and external pressures equal to 0 and 2 MPa, respectively cases 5 and 6, see Fig. 13.

The birdcaging configuration depends on the extent that the tape is allowed to yield, nonetheless the instability load is the same. To represent only one birdcaging, the tape is weakened in 1/30 of its total length. To better understand this situation case 5 was simulated again with two sections of weakened tape, with lengths 1/15 and 1/30 of total model length, see Fig. 14. When the tape weak section is larger, two birdcagings may occur but the critical load, i.e. the compressive response, is the same, see Fig. 15 that shows the axial load versus the end shortening for the two cases. It should be observed that the model does not take into account a progressive tape rupture.

The tape radial displacement along the pipe length on the instability onset is plotted in Fig. 16a,b for cases 5 and 6, where it is clearly observed that the wires displace radially. Before instability takes place

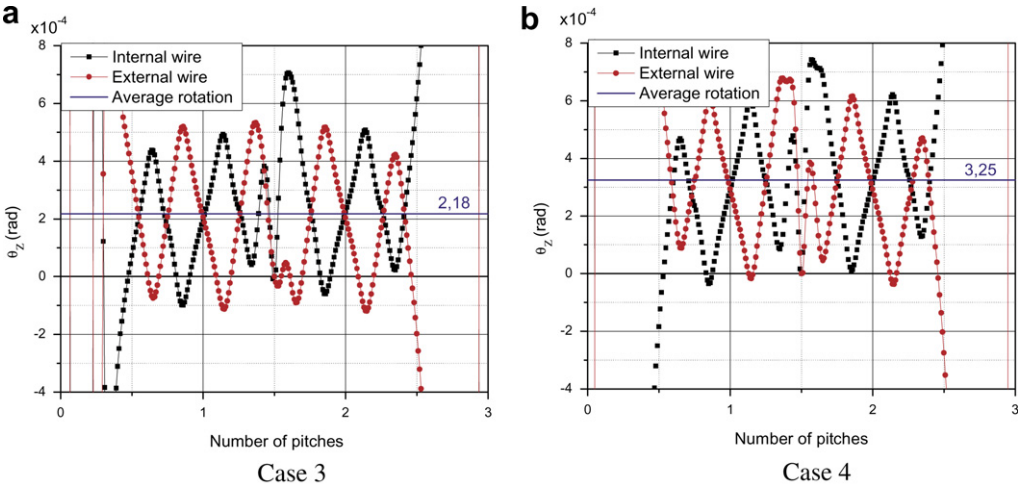

Fig. 12. Rotation around the *Z*-axis as a function of the model length.

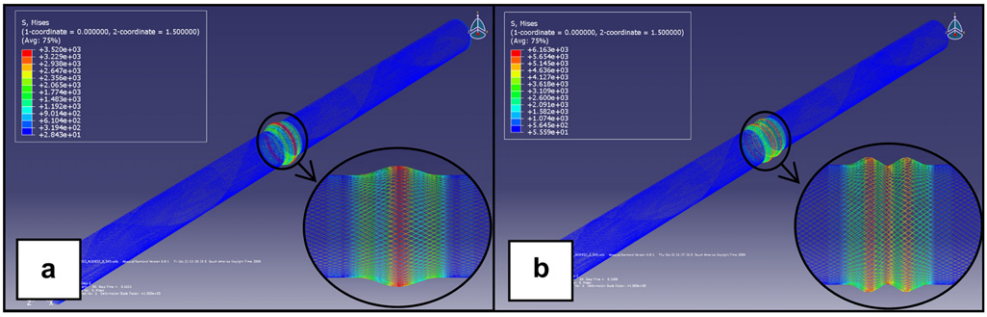

Fig. 13. Riser configuration with friction coefficient equal to 0.40 and external pressures equal to (a) 0 and (b) 2 MPa.

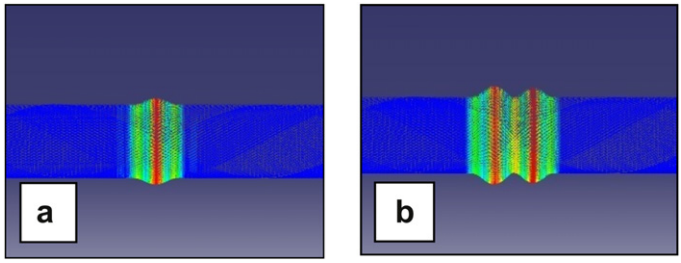

Fig. 14. Birdcaging configuration for case 5 for: (a) weakened tape 1/30 of model length; (b) weakened tape 1/15 of model length.

the radial displacement basically follows the axi-symmetric solution until the tape rupture capacity is reached.

Fig. 17 presents the axial force versus the radial displacement of the central node. When there is no external pressure (case 5) the central node displaces linearly as soon as an axial force is applied, until

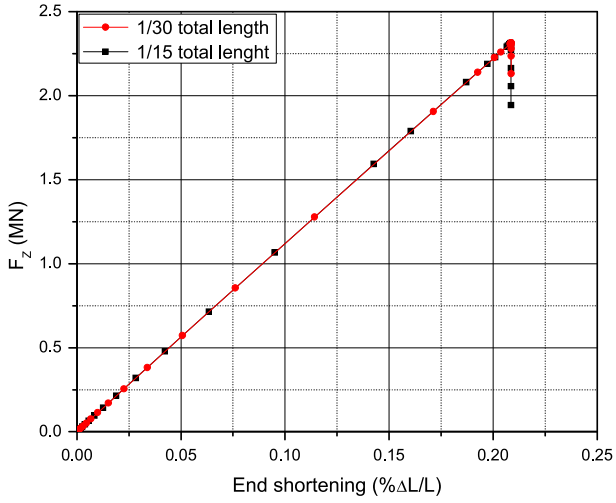

Fig. 15. Axial compressive force versus end shortening (case 5) when the weakened tape length is equal to 1/30 and 1/15 of the total model length.

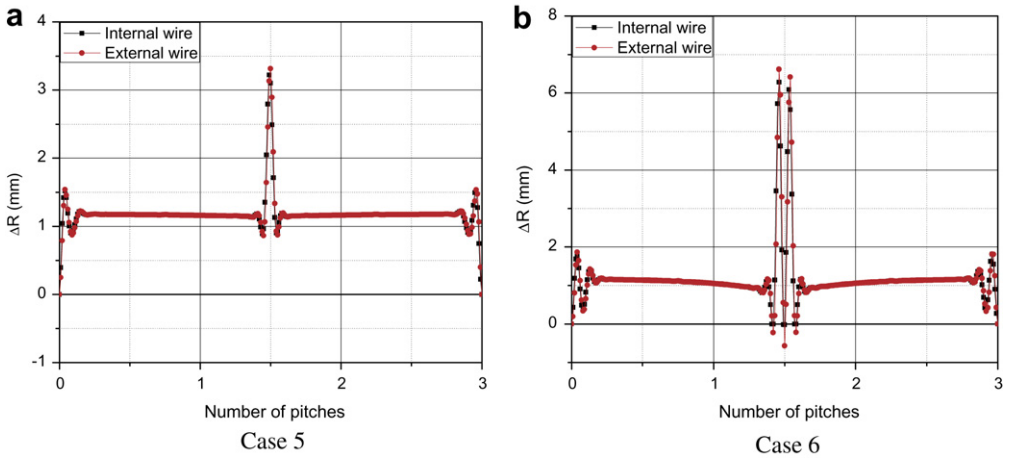

Fig. 16. Radial displacement as a function of the model length.

a maximum force, which corresponds to the birdcaging (tape failure!), is reached. When external pressure is applied (case 6), the radial displacement is initially zero until the external pressure is overcome and the wire expands radially. Observe that the inclinations are similar for cases 5 and 6 and that the birdcaging occurs for same radial expansion, in this case equal to 1.18 mm, which corresponds to the failure of the tape. Hence birdcaging is intimately connected to the failure of the birdcaging tape and the load can be also calculated analytically employing an axi-symmetric model. It should be emphasized that there is no gap and the anti-birdcaging tape perfectly supports the wires.

A possible influence of the internal radial stiffness is investigated in Fig. 18, which shows the reaction force in the central node of the foundations (N_{mol}) of the internal and external equivalent wires for case 6 as a function of the axial compressive force F_Z. Initially the internal foundation responds to the external pressure, but once this pressure is overcome the force drops to zero and the external foundation prevents the radial expansion, hence the internal stiffness does not interfere in the

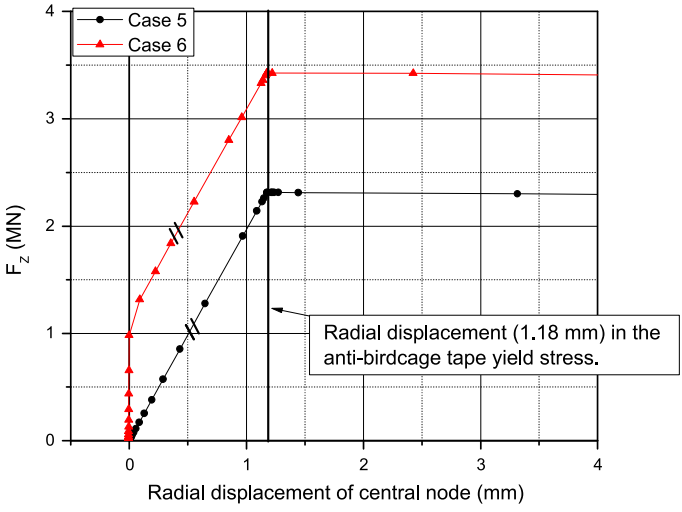

Fig. 17. Axial compression versus radial displacement of central node for cases 5 and 6.

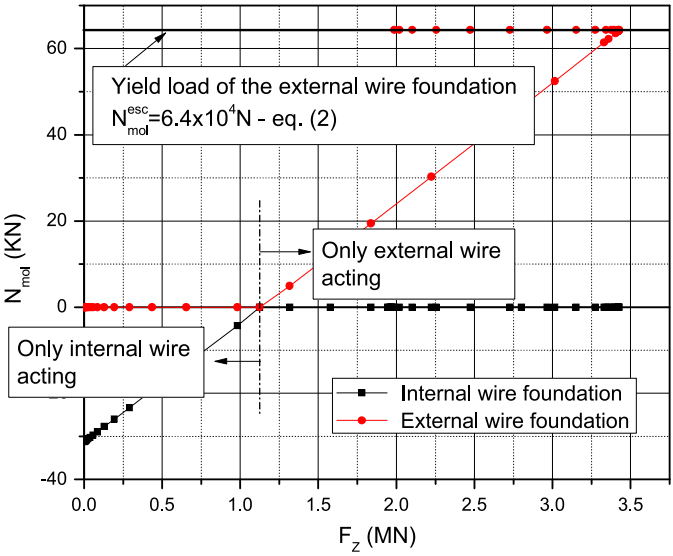

Fig. 18. Reaction forces for internal and external wires in the central node (case 6) as a function of the axial compressive force.

system behavior. It is also noted that when the structure instabilizes the axial compressive force suddenly drops when the tape fails.

Furthermore, it is important to investigate if this instability mode is purely radial or if it is accompanied by a combination of lateral displacements of the wires. Fig. 19 shows the wire rotation in the moment it instabilizes. It is seen that lateral displacement is also experienced.

3.4. Radial instability, MODE D

To observe this mode, cases 7 and 8 were chosen with friction coefficient 0.4 and external pressures equal to 6 and 8 MPa, respectively. The Fig. 20 illustrates the post-buckling configuration of the wires.

Fig. 21a,b shows the radial displacement as a function of the pipe length when the structure instabilizes for cases 7 and 8, where it can be clearly seen the "wrinkled" configuration of the wires. In this case wrinkling is due to spatial buckling of the wire on the elastic foundation before the anti-birdcage tape fails. It is important to emphasize that the yield stress was not reached in the armor wires.

The "wrinkling" is immediately alleviated the moment the tape fails. Fig. 22 presents the behavior for case 7 as the load is applied to the pipe. A radial scale factor equal to 20 was adopted to improve visualization of this behavior.

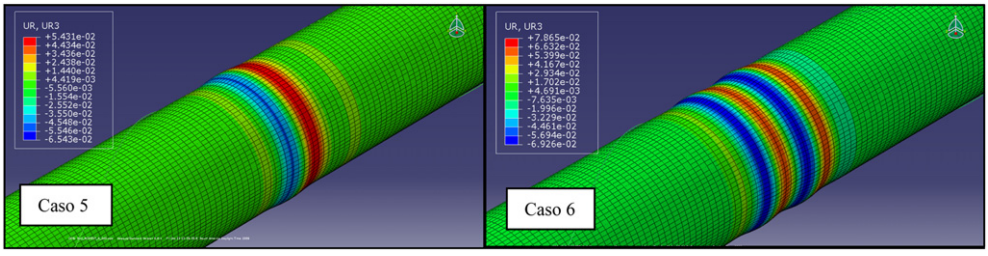

Fig. 19. Rotation around *Z* as a function of the model length (cases 5 and 6).

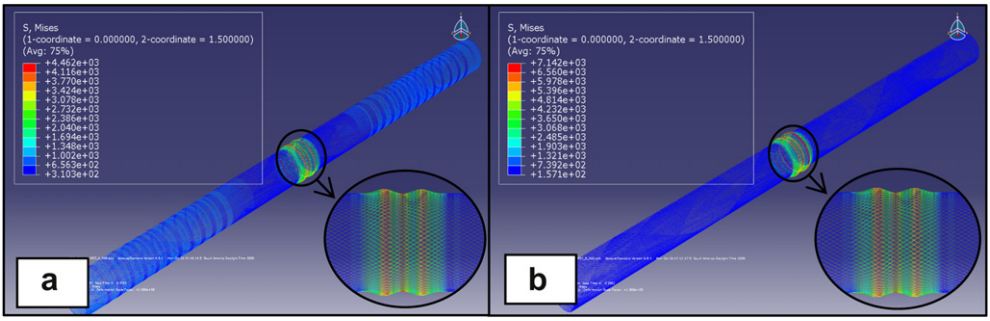

Fig. 20. Riser configuration with friction coefficient equal to 0.40 and external pressures equal to (a) 6 and (b) 8 MPa.

Fig. 23 shows the axial force as a function of the radial displacement at the central node for cases 7 and 8. The regions where wire "wrinkling" takes place are detached. In case 7 the wires overcome the external pressure, follow an axi-symmetric pattern and then "wrinkle". For case 8, on the other hand, the wires immediately "wrinkle" after the external pressure is overcome.

3.5. Final remarks

The possible instability modes have been discussed. It has been shown that the compressive behavior of flexible pipes strongly depends on the external pressure and friction coefficient between the armor wires. It is also important to verify if the instability is elastic or inelastic. To speed up the analysis the material was assumed linear elastic throughout the numerical simulations. Fig. 24 shows the von Mises stress (σ_{cr}^{Mises}) and the critical load (P_{cr}) for a central node versus the friction coefficient (μ_{mod}) when the external pressure is zero and 15 MPa. It is noted that from a friction coefficient approximately equal to 0.15 and external pressure equal to 15 MPa the wires reach a von Mises stress equal to 1100 MPa in the moment of instability, hence instability is inelastic. These cases are possible when the external layer is intact and the friction coefficient is high, and are nominated dry annulus instability.

When the external pressure is absent instability is elastic. Radial instability is only possible if friction coefficient is greater than 0.1. The anti-birdcaging tape prevents the armor wires from excessive radial

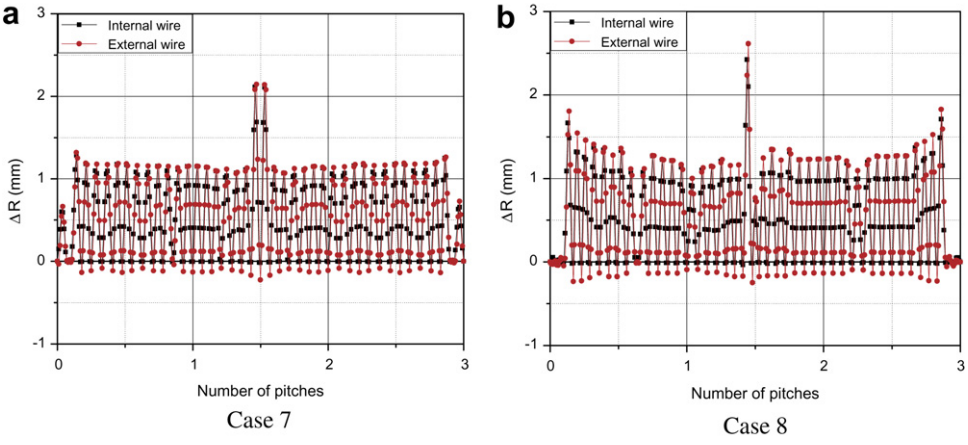

Fig. 21. Radial displacement as a function of the model length.

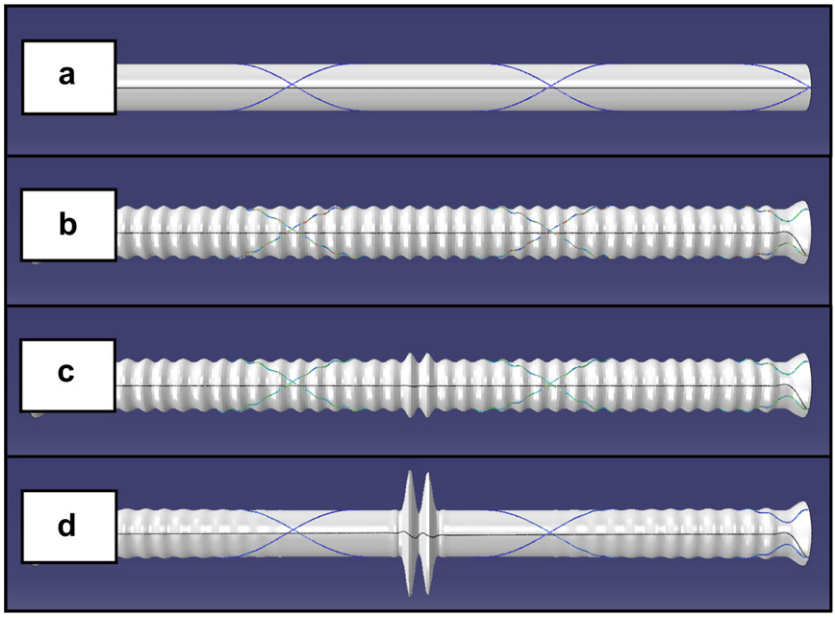

Fig. 22. Evolution of the pipe configuration (case 7): (a) $P = 0$, (b) $P <$ Pcr, (c) $P =$ Pcr and (d) $P >$ Pcr.

expansion. On the other hand, the friction coefficient reduces with seawater lubrication. Hence, radial instability is intimately associated with the rupture of the anti-birdcaging tape.

Fig. 25 shows that in the instability moment the distribution of the von Mises stress along the riser length when the external pressure is 15 MPa and the friction coefficient is equal to 0.15 is nearly constant except for the riser ends (because of the localized wire response), and is greater than the yield stress of the material.

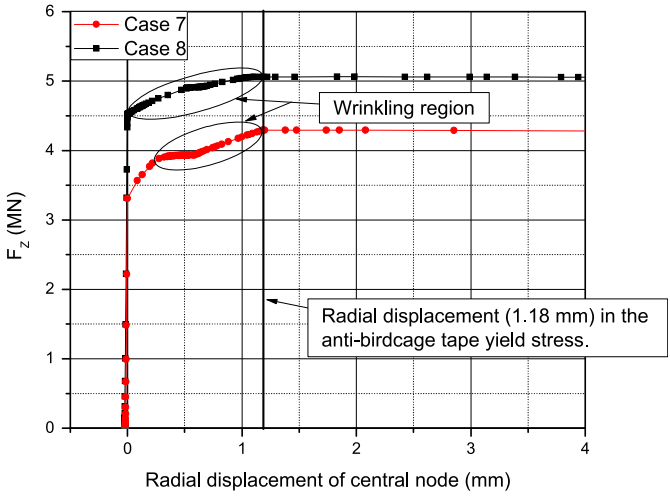

Fig. 23. Axial compression versus radial displacement of central node for cases 7 and 8.

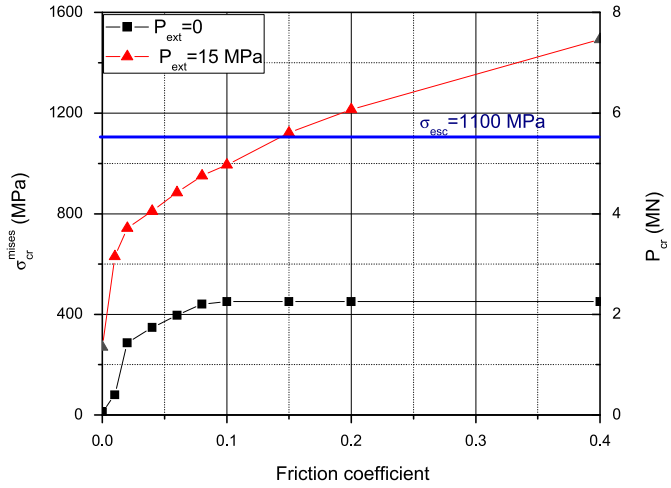

Fig. 24. von Mises stress (central node) and instability load versus friction coefficient when the external pressure is zero and 15 MPa.

The material regime in the moment of instability is highly dependent on the friction coefficient. In risers usually a polymeric tape is placed between the armor layers to reduce wear and a friction coefficient as low as 0.07 [12] may be assumed hence instability is expected to be elastic. In flowlines the direct contact between the steel armors may yield a friction coefficient as high as 0.8, hence instability is likely to be inelastic.

For the case study presented in this paper the armor wires contribute similarly to the flexible pipe axial and torsional stiffness hence the internal and external armor wires will always become instable simultaneously in both radial and lateral situations.

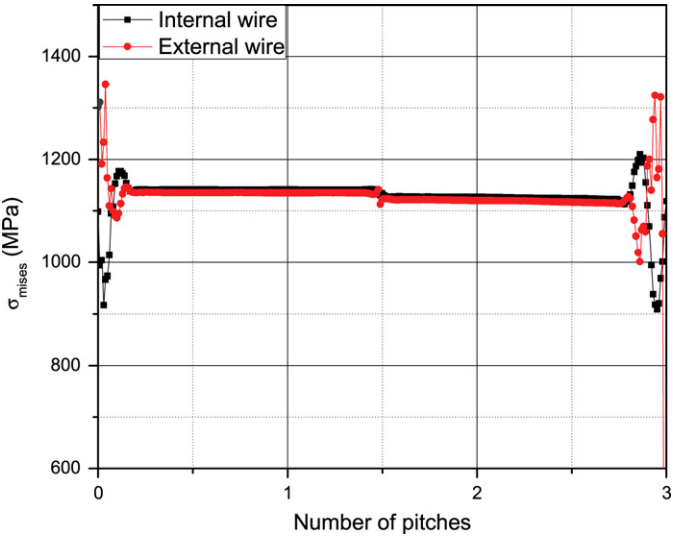

Fig. 25. von Mises stress along the riser length when the external pressure is 15 MPa and friction coefficient is equal to 0.15.

4. Conclusions

This work presents a non-linear finite element model to simulate the instability of unbonded flexible pipe wire armors subjected to axial compression. The model considers, in a simplified way, the contribution of all layers and assumes that each armor layer is represented by an equivalent wire. Hence the number of degrees of freedom is basically dependent on the refinement of the equivalent wires. It is important to comment that the geometrical imperfections and residual stresses were not introduced and are expected to reduce the critical load instability.

The effect of the friction coefficient between the armor wires and the external pressure on the instability load and mode has been extensively investigated via an ample parametric analysis. Both parameters influence the friction forces between the armor wires. The parametric study indicates that the most critical condition is experienced when the annular is flooded even though the net compressive force reduces in this case, because the friction coefficient substantially decreases (as compared to the dry annulus condition) and the hydrostatic pressure does not support the wires.

The instability load and the failure mode strongly depend on the friction coefficient and external pressure. Four instability modes have been identified, two related to lateral instability and the other two related to radial instability. In the lateral instability modes the anti-birdcaging tape is intact and the armor wires may instabilize independently or not, respectively for low and high friction forces. The radial instability modes may be related to the anti-birdcaging tape failure and elastic foundation buckling. In both cases coupled lateral displacement is experienced by the wires. When birdcaging occurs the inner most layers (interlocked carcass, pressure armor and plastic sheaths) do not play any role. It was observed that the failure tends to be inelastic when the pipe annular is dry but in wetted conditions instability is probably elastic. The independent lateral instability mode is unlikely for flexible pipes when the axial and torsional stiffness of the wire cross-section are similar.

Acknowledgments

The authors acknowledge the support of the National Council of Scientific and Technological Development (CNPq) for this work.

References

[1] Api RP 17B. Recommended practice for flexible pipe. 2nd ed. Washington: American Petroleum Institute; 2008.
[2] Bectarte F, Coutarel A. Instability of tensile armour layers of flexible pipes under external pressure. In: Proceedings of the OMAE2004 conference; 2004. Vancouver, Jun.n.51352.
[3] Braga M. Instabilidade das Armaduras de Tração de Linha Flexíveis. Tese de D.Sc. Rio de Janeiro, Brasil: COPPE/UFRJ; 2003.
[4] Costello GA. Theory of wire rope. In: Mechanical engineering series. 2nd ed. New York: Springer-Verlag Inc.; 1997.
[5] Custódio AB. Modelo Analítico para Avaliação da instabilidade nas Armaduras de Dutos Flexíveis. Tese de D.Sc. Rio de Janeiro, RJ, Brasil: COPPE/UFRJ; 2005.
[6] ABAQUS theory and user's manual, version 6.8. Pawtucket, RI, USA: Hibbitt, Karlsson and Sorensen. Inc.; 2001.
[7] Novitsky A, Sertã S. Flexible pipe in Brazilian ultra-deepwater fields – a proven solution. In: Proceedings of the 14th deep offshore technology; 2002. Riser Technology Symposium, New Orleans, Nov.
[8] Rizzo NAS. Análise da instabilidade das armaduras de dutos flexíveis pelo método de elementos finitos. Dissertação de M. Sc. Rio de Janeiro, RJ, Brasil: COPPE/UFRJ; 2010.
[9] Sousa JRM. Análise Local De Linhas Flexíveis Pelo Método Dos Elementos Finitos. Tese de D.Sc. Rio de Janeiro, RJ, Brasil: COPPE/UFRJ; 2005.
[10] Stump D, Heidjen G van der. Birdcaging and collapse of rods and cables in fixed-grip compression. International Journal of Solids and Structures 2001;38:4265–78.
[11] Tan Z, Loper C, Sheldrake T. Behavior of tensile wires in unbonded flexible pipe under compression and design optimization for prevention. In: Proceedings of the OMAE2006 conference; 2006. Hamburg, Jun.
[12] Troina LMB, Rosa LFL, Viero PF, Magluta C, Roitman N. An experimental investigation on the bending behaviour of flexible pipes. In: Proceedings of the OMAE2003 conference; 2003. Cancun, Jun.
[13] Witz JA. A case study in the cross-section analysis of flexible risers. Marine Structures 1996;9:885–904.
[14] Zhang Y, Chen B, Qiu L, Hill T, Case M. State of the art analytical tools improve optimization of unbonded flexible pipes for deepwater environments. In: Proceedings of the 37th offshore technology conference (OTC), OTC-15169; 2003. Houston, May.